J. Fluid Mech. (1974), *vol.* 66, *part* 1, *pp.* 159–176
Printed in Great Britain

The near wall jet of a normally impinging, uniform, axisymmetric, supersonic jet

By J. C. CARLING† AND B. L. HUNT
Department of Aeronautical Engineering, University of Bristol, England

(Received 11 February 1974)

The near wall jet produced by directing a uniform axisymmetric jet of air normally onto a large flat plate has been investigated experimentally and theoretically for four jets in the Mach number range 1·64–2·77. Detailed measurements of the surface pressure and shadowgraph and surface flow pictures are presented. The results show that the mechanism which mainly determines the supersonic near wall jet is the jet-edge expansion and its reflexions from the sonic line and the wall-jet boundaries. The near wall jet is found to consist of an alternating series of expansion and recompression regions whose strengths depend on the jet Mach number and decay with distance. At Mach numbers of 2·4 and above, shock waves are observed in the first recompression region and at a Mach number of 2·77 the boundary layer separates locally. Further out, viscous effects become increasingly important and a constant-pressure shear flow is established at a distance which increases with jet Mach number. The application of the method of characteristics in an approximate manner reproduces a number of the features of the near wall jet which are observed experimentally.

Pressure distributions obtained in the shock layer show that a stagnation bubble can occur and that its occurrence depends on factors such as the flow upstream of the nozzle. The wall-jet region is found to be largely independent of whether or not a bubble occurs in the shock layer.

1. Introduction

The impingement of a uniform, axisymmetric, supersonic jet upon a flat surface arranged perpendicular to the axis produces a curved shock wave which spans the jet and is convex upward. This and other features of the flow are shown in figure 1. Below the shock wave, the flow is subsonic. As the shock-layer fluid moves radially outward, its velocity increases and a sonic line occurs in the region below the jet edge. Thereafter the fluid enters a wall jet which is initially supersonic. However, a shear layer grows along the constant-pressure upper boundary of this wall jet and a boundary layer along the solid surface; these viscous layers must eventually merge and reduce the wall-jet velocities to subsonic values.

The subsonic impingement region has been studied by Gummer & Hunt (1971), who presented theoretical and experimental results for surface pressures out as

† Present address: Department of Ceramics, Glasses and Polymers, University of Sheffield.

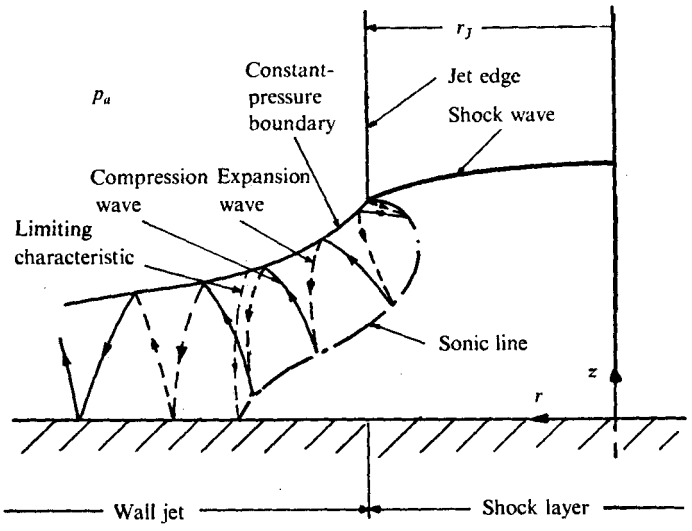

FIGURE 1. The shock layer and transonic zone at low jet Mach number ($M_J \lesssim 1{\cdot}6$).

far as the surface sonic point and for shock shapes. Four jet Mach numbers were studied in the range 1·64–2·77. They also used qualitative theoretical arguments to give a description of the rather complex flow which occurs in the neighbourhood of the sonic line. In another piece of work on the same rig, Greenwood (1969) observed the formation of ice and oil rings on the solid surface in the wall-jet region. This observation, together with Gummer & Hunt's description of the sonic-line region, suggested that the near wall jet merited further investigation.

This paper describes a study of the wall jets from the four jets used in the earlier investigations; the Mach numbers are 1·64, 1·84, 2·41 and 2·77. Surface flow pictures, shadowgraph photographs and surface pressure measurements were all obtained in the experimental work, while an approximate application of the method of characteristics is presented in support of the flow model used to interpret the experimental results. This flow model is based on Gummer & Hunt's (1971) description of the flow near the sonic line; this description is therefore summarized in the next section.

2. The flow near the sonic line according to Gummer & Hunt (1971)

This section gives a brief account of certain arguments which lead to the flow model used in this work. Gummer & Hunt's paper should be referred to for details. An earlier paper by Henderson (1966) is also relevant.

In this treatment, it is assumed that the flow in the shock layer and near the sonic line can be treated as inviscid. Now, the principal factor which determines the inviscid flow near the sonic line is the behaviour of the jet-edge streamline, which must remain at constant pressure while turning outwards. The main shock extends to the jet edge and produces some outward deflexion. However, the shock also produces a rise in pressure and, consequently, the jet-edge streamline im-

mediately returns to ambient pressure by means of a centred expansion which produces a further outward deflexion. The need for this centred expansion means that the edge streamline must be at least sonic downstream of the shock and, hence, that the sonic line must intersect the shock at, or inboard of, the jet edge. The waves from the centred expansion undergo a series of reflexions, first at the sonic line and subsequently at the constant-pressure boundary and at the solid surface; it is these waves which determine the main features of the inviscid wall-jet structure.

The approximate location and shape of the sonic line can be inferred as follows. If the sonic line is to terminate on the shock wave at a point inboard of the jet edge, it is necessary for expansion waves to originate on the upper part of the sonic line and to intersect the outer part of the shock wave, so weakening it. Hunt (1972) has shown that this is only possible if the flow is non-homentropic. The flow within the shock layer is homentropic for low jet Mach numbers but is otherwise non-homentropic. It follows that the sonic line must terminate at the edge of the shock wave if the jet Mach number is near unity but can terminate inboard of the edge in the case of higher jet Mach numbers. Gummer & Hunt (1971) also point out that a flow singularity is avoided at the higher jet Mach numbers, if the sonic line is inboard of the jet edge. The extent of any inward displacement which occurs is limited by the strength of the expansion waves produced by the sonic line, and, at least in principle, by the requirement that at least one characteristic from the jet edge must reach the sonic line in order that the subsonic region can be influenced by the scale of the jet. The only information on the location of the foot of the sonic line comes from experimental evidence which shows that the sonic point on the surface is slightly outboard of the line of the jet edge but moves towards the jet edge as the jet Mach number increases. The slope of the sonic line at the shock wave can be found from results† presented by Hayes & Probstein (1966, p. 396). It is not possible to calculate the angle of the sonic line at the solid surface without knowing the radial velocity gradient. However, it can be shown that the sonic line is inclined upstream as it leaves the surface but that its inclination to the surface tends to 90° as the jet Mach number approaches unity.

The angle of the edge streamline after the centred expansion and the angular region occupied by the initial part of the centred expansion can be easily calculated. These quantities, together with the information about the sonic line which has just been described, enable the wave structure just downstream of the sonic line to be sketched. Figures 1, 2 and 3 contain such sketches for the approximate jet Mach number ranges 1–1·6, 1·6–2·8 and $> 2{\cdot}8$, respectively. The main features to note at this stage are the changing shape of the sonic line and that at low Mach numbers the centred expansion waves can be reflected several times between the constant-pressure boundary and the sonic line, whereas at higher jet Mach numbers the higher Mach number and greater deflexion of the constant-pressure boundary give rise to expansion waves which reach the solid surface directly. In all cases, there are expansion waves which leave the solid surface and

† Hayes & Probstein's results assume planar flow. However, calculations in which the effect of axisymmetry was estimated suggest that its influence is not large.

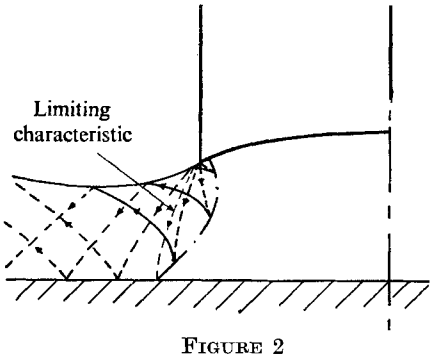

FIGURE 2

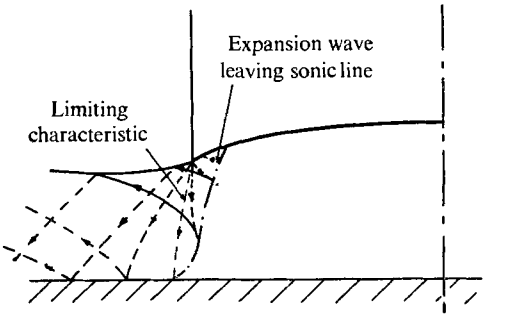

FIGURE 3

FIGURE 2. The transonic zone at moderate jet Mach number ($1{\cdot}6 \lesssim M_J \lesssim 2{\cdot}8$).
FIGURE 3. The transonic zone at high jet Mach number ($M_J \lesssim 2{\cdot}8$).

which will therefore be returned as compression waves by the constant-pressure boundary; the subsequent part of an inviscid wall jet will contain alternating sections of expansion waves and compression waves.

3. Experimental apparatus

The supersonic jets were produced by three axially symmetric, contoured, convergent–divergent nozzles of Mach numbers 1·64, 2·41 and 2·77 which had been used earlier by Gummer & Hunt (1971). The throat diameter of these nozzles was 12·7 mm. A fourth nozzle used by Gummer & Hunt of Mach number 1·84 was also used in some of the work. Unfortunately, this nozzle was damaged before the tests were completed. A replacement was made but a slight error in manufacture occurred and the resulting jet was found to have a mean Mach number of 1·76. Judging by the results, it does not appear that the difference between the original nozzle and its replacement is very significant in the present context.

The uniformity of the jets had been investigated earlier by traversing with a Pitot tube. The Mach number variation in the inviscid part of the jet was then determined, assuming a uniform upstream stagnation pressure. The $M_J = 2{\cdot}77$ nozzle showed the worst variation, of about 4 %. The variations in the other nozzles are within 2 % of the nominal values.

Two different rigs were used in the work and, although they both served the same function of supplying air at the appropriate stagnation pressure to the nozzle, the results showed that they did influence the impingement flow, although probably only in the shock-layer region. Some details of the rigs will therefore be given here. In the first rig (referred to here as rig I), air at up to 30 bar and the ambient stagnation temperature was drawn from the Department's high pressure main through approximately 3·5 m of 2·5 cm bore steel pipe into which the convergent–divergent nozzle was screwed. A manually operated gate valve was used to reduce the air pressure to the appropriate stagnation pressure. The particular running conditions were set to give the ambient pressure according to a static pressure tapping located close to the nozzle exit plane; the stagnation pressure at the nozzle entry was monitored on a Budenberg test gauge. The

second rig (referred to here as rig II) is of more elaborate design. The main supply pipes are 15 cm in diameter and lead from the high pressure main to a 'Camflex' reducing valve which can be operated either manually or automatically by means of a 'Wizard' pressure controller. A manually operated globe isolating valve is also installed. After passing through the valves, the air enters a settling chamber of diameter 15 cm which includes a number of smoothing gauzes. The air leaves the settling chamber through a smooth contraction leading to the nozzle. The settling-chamber pressure was monitored on a Budenberg test gauge and running conditions established so as to give zero indicated exit-plane gauge pressure. In both rigs, the impingement plate was set perpendicular to the jet axis and at a known distance from the nozzle exit by means of slip gauges. The nozzle-to-plate spacing was kept small (in most cases it was approximately equal to the radius of the jet) in order to minimize the influence of the shear layer which exists at the edge of the jet.

Surface pressures were measured using rig II. The method employed was to traverse a single static tapping of diameter 0·75 mm mounted in the centre of an aluminium disk of diameter 20 cm. The disk in turn was set flush with the top surface of a 25 cm square steel plate. The plate was mounted on a workshop machine table with compound cross-slides which enabled very accurate location of the pressure tapping. The accuracy of location from a given reading using this method is estimated to be $\pm$ 0·025 mm. A second static tapping was located 7 cm from the centre of the disk along one of the slide axes and used to obtain values at relatively large distances from the centre. The particular tapping point which was in use at any time could be connected at will to either a 0–13 bar Budenberg Test Gauge or a 65 cm high mercury U-tube. This simple system proved reliable and accurate in practice, as the details on the pressure distributions (figures 8(*a*)–(*d*)) confirm.

Surface flow visualization was carried out on rig I. The visualization was carried out by painting the solid surface with a mixture of approximately 50 ml of heavy paraffin with 40 g of orange Dayglo powder. The jet was then rapidly brought to its designed condition and, when the paint had established an unchanging pattern (this normally took approximately 1 min), the jet was shut off: the gate valve enabled an almost instantaneous cut-off in the air supply to be achieved with no disturbance of the Dayglo patterns. The patterns were then photographed off the rig under ultra-violet light.

A focused shadowgraph system was used to obtain photographs of the main shock and of certain waves in the wall-jet region. This system was similar to that used by Gummer & Hunt (1971) except that the arrangement of the rigs used here enabled the astigmatism to be eliminated. Photographs were taken on both rigs.

4. Experimental results

4.1. *The shock layer*

The main objective of the work was to examine the wall-jet region. However, surface pressure measurements were also taken in the shock layer. These pressure distributions turned out to have a surprising form; they may have an influence

on the interpretation of the wall-jet results and, in any case, are of interest in their own right; they are therefore presented and discussed in this section.

Figures 4 (*a*)–(*d*) show the pressure distributions in the shock layers of the four impinging jets for a nozzle-to-plate distance approximately equal to the jet radius. The pressures p have been non-dimensionalized with respect to the stagnation pressure behind a normal shock at the Mach number of the free jet and the radial distance r with respect to the nozzle exit radius. Also shown on the figures are the results obtained by Gummer & Hunt (1971). The results of the current series of tests were obtained along two perpendicular diameters: it can be seen that the flow is remarkably symmetric in the wall jet but that it may be asymmetric in the shock layer.

The most notable feature of the distributions is that, over the central region of the 1·64, 2·41 and 2·77 nozzles, the pressure is almost constant at a value markedly below the normal-shock recovery pressure and rises to a maximum (although not to the normal-shock value) at a non-dimensional radius somewhat less than unity. Gummer & Hunt (1971) reported similar behaviour in the case of the $M_J = 2{\cdot}41$ nozzle at a plate-to-nozzle displacement of 0·84 times the jet radius. They interpreted this distribution as indicating the presence of a bubble of slowly recirculating fluid in the shock layer; the present results suggest the same interpretation. Perhaps the most remarkable aspect of these results, however, is that all the rest of Gummer & Hunt's results, both with the 2·41 nozzle at other displacements and with the other nozzles, contained no evidence of a bubble (as can be seen from the distributions reproduced in figure 4 of this paper) despite the fact that their results at Mach numbers of 1·64, 2·41 and 2·77 were obtained with the same nozzles as were used in this work. Since the mechanism which determines the occurrence of the bubble is not known, it is difficult to decide which of the differences between the conditions of the present work and the conditions of Gummer & Hunt's work are relevant. The only two differences which seem to be worth stating are that different rigs were used and that the plate used in the present work was highly polished, whereas Gummer & Hunt's plate was not. In Gummer & Hunt's rig, the air was taken from the high pressure main through a short (1 m) length of 3·8 cm diameter pipe and fed to the nozzle with no settling chamber.

A detailed discussion of the bubble is not necessary as far as the wall jet is concerned but, having mentioned this interesting phenomenon, it would, perhaps, be unreasonable if a brief summary of the other relevant evidence were not given, even though it tends to raise more questions than it answers. Limited attempts were made to establish a flow without the bubble by changing the plate displacement and by temporarily opening the central pressure tapping to the atmosphere in the hope that this would drain the bubble and allow an unseparated flow to become established. Neither method was successful. Other nominally uniform jets used on rig II gave pressure distributions which showed no evidence of a bubble: for example, the pressure distribution from the 1·76 nozzle, shown on figure 4 (*b*), contains a slight irregularity within the shock layer but achieves normal-shock recovery at the origin and it is unlikely that a bubble is present in this case. Finally, bubbles have been observed in the shock layers of various

non-uniform impinging jets on the rig used by Gummer & Hunt (see Gummer 1968) and on a totally different rig (see Donaldson & Snedeker 1971). Attempts are currently being made to discover the mechanism which determines the occurrence of these bubbles.

Although a detailed study of the shock-layer flow is not appropriate here, nonetheless the following aspects of the existence of the two possible flows are important as far as this work is concerned. The results presented here contain evidence collected on two different rigs. Two questions arise, namely, whether or not the shock-layer flow for each jet was in the same state on both rigs and, in any case, whether the state of the shock-layer flow has a significant effect on the wall jet. As far as the flows occurring on the two rigs are concerned, none of the Dayglo and shadowgraph pictures obtained on rig I shows any evidence of a bubble, while the pressure distributions from rig II show that bubbles occurred for the $M_J = 1{\cdot}64$, 2·41 and 2·77 nozzles. The shock layers of these jets therefore depend on the rig. The 1·76 nozzle on rig II appears to operate without a bubble and therefore in the same state as the 1·84 nozzle on rig I. A comparison of the unseparated pressure distributions obtained by Gummer & Hunt with the present results is made in figure 4 and shows good agreement outside the bubble. (Note also that the pressure distribution for the 1·76 nozzle agrees well with that for the 1·84 nozzle.) Further, a shadowgraph picture showing an internal-shock/boundary-layer interaction in the near wall jet was obtained on rig II for the 2·77 nozzle (figure 5, plate 1†) and may be compared with a similar picture for the same nozzle taken on rig I (figure 7*c*, plate 4). No differences can be detected in the position and nature of the interaction. The evidence therefore suggests strongly that the wall-jet flow is not significantly affected by the presence of a bubble in the shock layer; this is consistent with the notion, expressed earlier, that the wall-jet flow is mainly determined by the jet-edge expansion and its interaction with the sonic line and wall-jet boundaries.

4.2. *Presentation and discussion of the wall-jet results*

Photographs of the Dayglo surface patterns obtained at plate displacements of about one jet radius with the $M_J = 1{\cdot}64$, 1·84, 2·41 and 2·77 nozzles on rig I are shown as figures 6 (*a*)–(*d*) (plates 2 and 3) respectively. A problem encountered on rig I was that the pressure drop down the long narrow supply pipes prevented the designed stagnation pressure from being achieved with the 2·77 nozzle. However, the static pressure at the nozzle exit was too low by only about 10 %. Also, pressure distributions were obtained on rig II with this amount of overexpansion and were found to be indistinguishable from pressure distributions measured with the correctly expanded jet. As far as the photographs themselves are concerned, a light colour indicates the presence of Dayglo paint and the darkest areas are those from which paint has been removed. The most striking features are the symmetric rings of Dayglo paint which occur in each case, starting at a point which is of the order of twice the jet radius from the axis. As many as six rings can be distinguished at the higher Mach numbers, with the innermost ring

† The sharply peaked shock shape seen in this picture is characteristic of the shapes observed when bubbles are present.

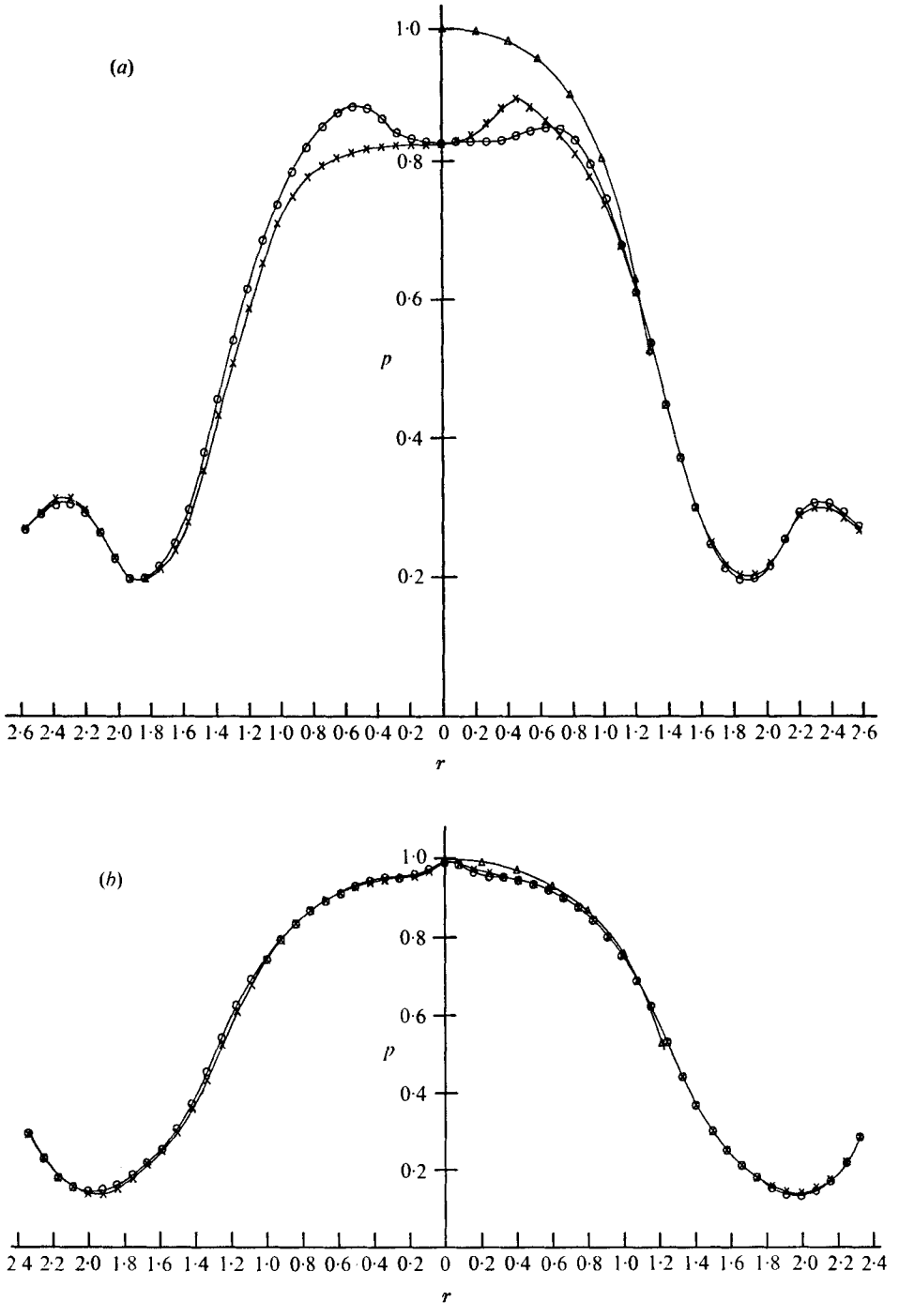

FIGURES 4 (*a*, *b*). For legend see facing page.

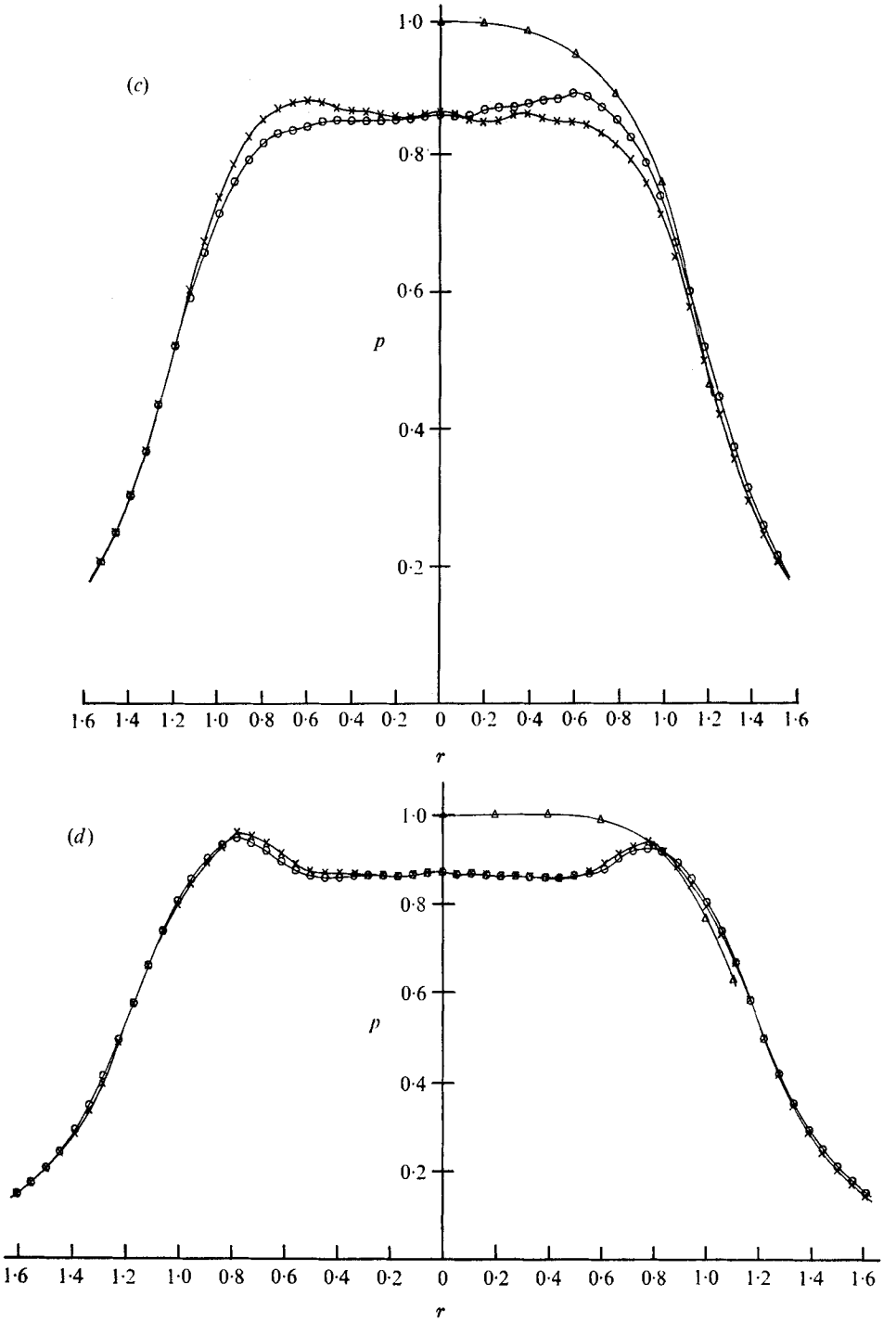

FIGURE 4. Shock-layer surface pressures for (*a*) $M_J = 1{\cdot}64$, (*b*) $M_J = 1{\cdot}76$, (*c*) $M_J = 2{\cdot}41$ and (*d*) $M_J = 2{\cdot}77$. The pressures are non-dimensionalized with respect to the nominal free-jet Pitot pressure and the radial co-ordinate with respect to the jet radius. ×, ○, current results along perpendicular diameters; △, Gummer & Hunt's results.

sometimes having a complex structure. The appearance of the pictures for the $M_J = 2{\cdot}41$ and 2·77 jets, particularly, is slightly marred by the effect of small oil droplets contained in the air. The oil, however, does not seriously diminish the usefulness of the pictures. A much more detailed interpretation of the significance of the Dayglo rings will be given in §4.3.

The Dayglo rings were believed to be due to the system of waves in the near wall jet which originate in the jet-edge expansion in the manner described in §2. Shadowgraph pictures were therefore taken on rig I of the shock-layer and near-wall-jet regions. The $M_J = 1{\cdot}84$ nozzle had been damaged at this time and no shadowgraph of this flow was taken. However, figures 7 (*a*)–(*c*) (plate 4) show the shadowgraphs obtained for the other three nozzles, the 2·77 nozzle again being operated very slightly overexpanded. The following points may be made about these pictures. In the $M_J = 1{\cdot}64$ wall jet, Mach waves can be seen, produced by surface imperfections, but there do not appear to be any strong waves present. In contrast, the 2·41 and 2·77 nozzle shadowgraphs contain clear evidence of internal shock waves; these shadowgraphs are interpreted as showing a shock/boundary-layer interaction consisting of an oblique shock, followed by a separation or thickening of the boundary layer, and a reattachment shock. Although the free-shear-layer upper boundary of the wall jet is not clearly defined on the shadowgraphs, it can nonetheless be seen that the wall-jet thickness decreases rapidly in the vicinity of the shock waves. This, coupled with the thickening of the boundary layer which must result from the shock/boundary-layer interaction, will considerably increase the influence of shear flow in the subsequent parts of the wall jet: this may account for there being no visible inviscid wave structure in the outer part of the wall jet.

Figures 8 (*a*)–(*d*) show the pressure distributions obtained on rig II for the wall-jet regions of the four jets. It will be seen that the measurements show details of a complex variation with virtually no scatter and very high resolution (a difference in r on the figures of 0·1 corresponds to less than 1 mm on the plate). The distributions all show the initial acceleration of the fluid near the jet edge followed by a region in which the pressure undergoes a spatially periodic variation of decaying amplitude and subsequently approaches atmospheric pressure. The outer limit of the periodically varying region increases with jet Mach number M_J from about 4 times the jet radius at $M_J = 1{\cdot}64$, when three pressure maxima occur, to 8·5 jet radii at $M_J = 2{\cdot}77$, when six pressure maxima can be distinguished. The periodic variations in pressure are consistent with the alternating expansion and compression regions predicted by the qualitative study of the inviscid flow given in §2. The decay of the pressure variations and the return to atmospheric pressure are taken to be due to the spread of the turbulent shear flows from the two boundaries of the flow. The regions of pressure rise and fall of the 1·64 and 1·76 wall jets are smooth and consistent with continuous recompression and expansion and therefore with the shadowgraph of the 1·64 jet, which does not contain any strong waves. The second and subsequent cycles of the $M_J = 2{\cdot}41$ distribution are also smooth, the corresponding cycles of the $M_J = 2{\cdot}77$ results slightly less so. However, the first pressure rise of the $M_J = 2{\cdot}77$ pressure distribution contains considerable local variation. The visible wave phenomena from

the shadowgraph of this wall jet have been reproduced on the pressure distributions and it can be seen that the first wave and its subsequent interaction with the boundary layer coincide virtually exactly with a sharp pressure rise and a subsequent constant-pressure region. The constant pressure shows that the boundary layer must be separated in this region. The position of the second wave seen in the shadowgraph agrees with a subsequent sharp rise in the pressure distribution. The fall in the pressure gradient behind this shock cannot be unambiguously connected with any feature visible on the shadowgraph but is probably due to a rapid thickening of the boundary layer brought about by the second shock. The first pressure rise of the $M_J = 2{\cdot}41$ wall jet is not structured in as complex a way as that of the 2·77 wall jet. However, a region of much reduced pressure gradient exists in the same position as the shock/boundary-layer interaction which is visible on the shadowgraph. In this case, the pressure variation suggests that the boundary layer may not separate but probably thickens very rapidly instead.

4.3. *Interpretation of the Dayglo patterns*

The Dayglo rings of figure 6 have been represented along the abscissae of figure 8 by contours indicating the relative thicknesses of the Dayglo deposits, as far as they can be inferred from the photographs. This, clearly, is not an exact process and this alone is a reason for not demanding a very close agreement between the contours and the pressure distributions.

The main features arising from a comparison of the Dayglo contours and the pressure distributions are as follows. There is a Dayglo deposit corresponding to the pressure minimum of every cycle except the last, weakest cycles. The deposits are disposed roughly symmetrically around the second and later minima but commence at the minimum point and extend over much of the region of pressure rise in the case of the first minimum. The Dayglo deposits and the pressure distributions in the region of the first minima of the higher Mach number jets both show some complexity of structure.

Precisely what determines the Dayglo patterns is not known but the following is an attempt to explain their main features. The paint will be removed by the shearing action of the air in regions where the wall shear stress is high: this accounts for the removal of the paint from the shock-layer region. However, the material is viscoplastic and can withstand a certain level of shear stress without flowing, thus accounting for the uniform deposits found in the outer regions where the velocities are lower. The shear stress is also reduced in the presence of an adverse pressure gradient, which accounts, at least in part, for the deposits occurring downstream of the pressure minima. Another factor which may help to maintain deposits in regions of increasing pressure is that the resultant pressure force on the small but finite inner and outer faces of the Dayglo layer will act in an inward direction, in opposition to the shearing force. These factors do not explain the deposits which are found ahead of the minima, where the shear stress is increased by the pressure gradient and the resultant pressure force is directed outwards. In this case, the explanation is probably that the deposits which occur in the adverse pressure gradient, downstream of the minima, prevent

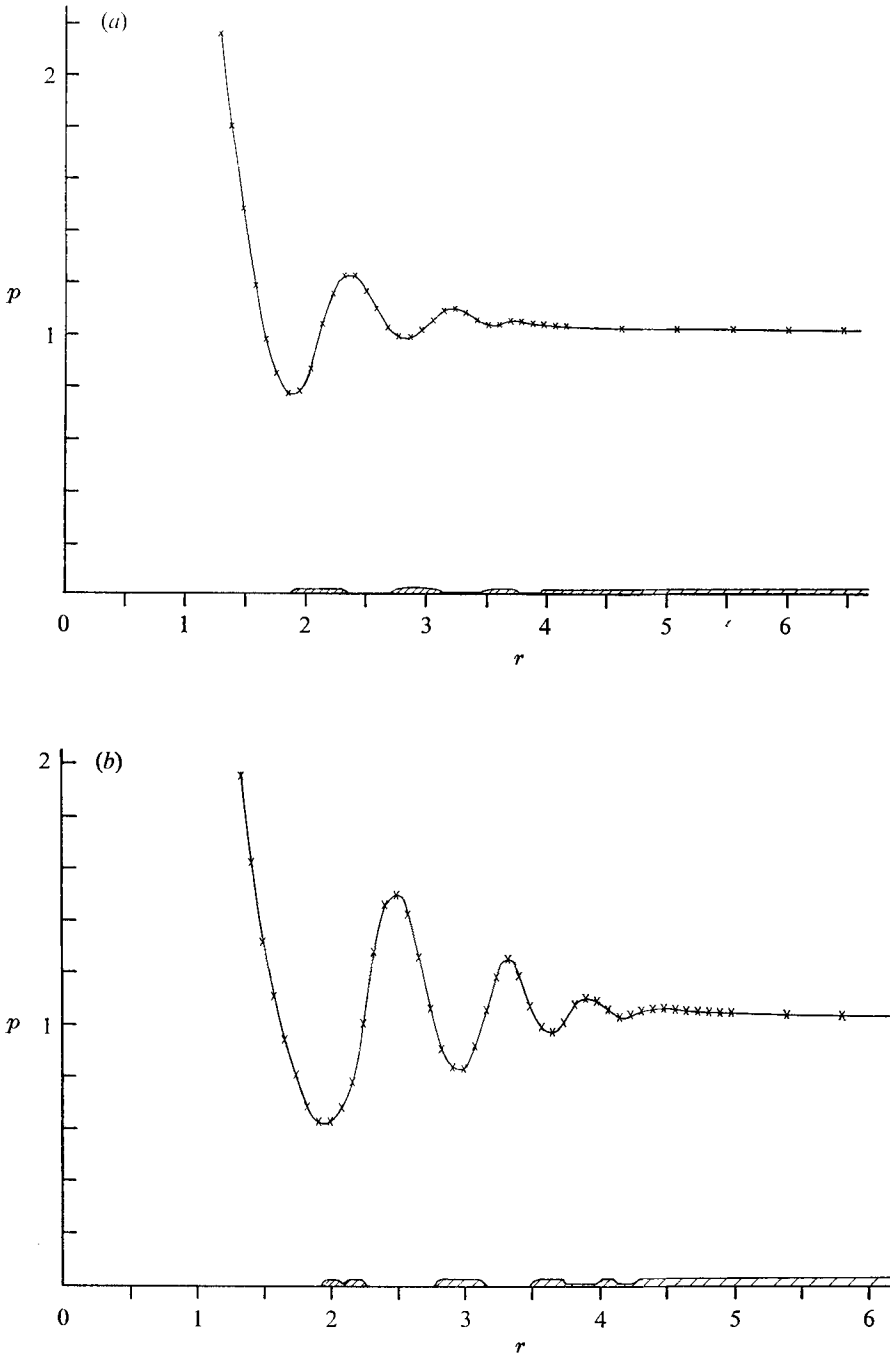

FIGURES 8 (*a*, *b*). For legend see facing page.

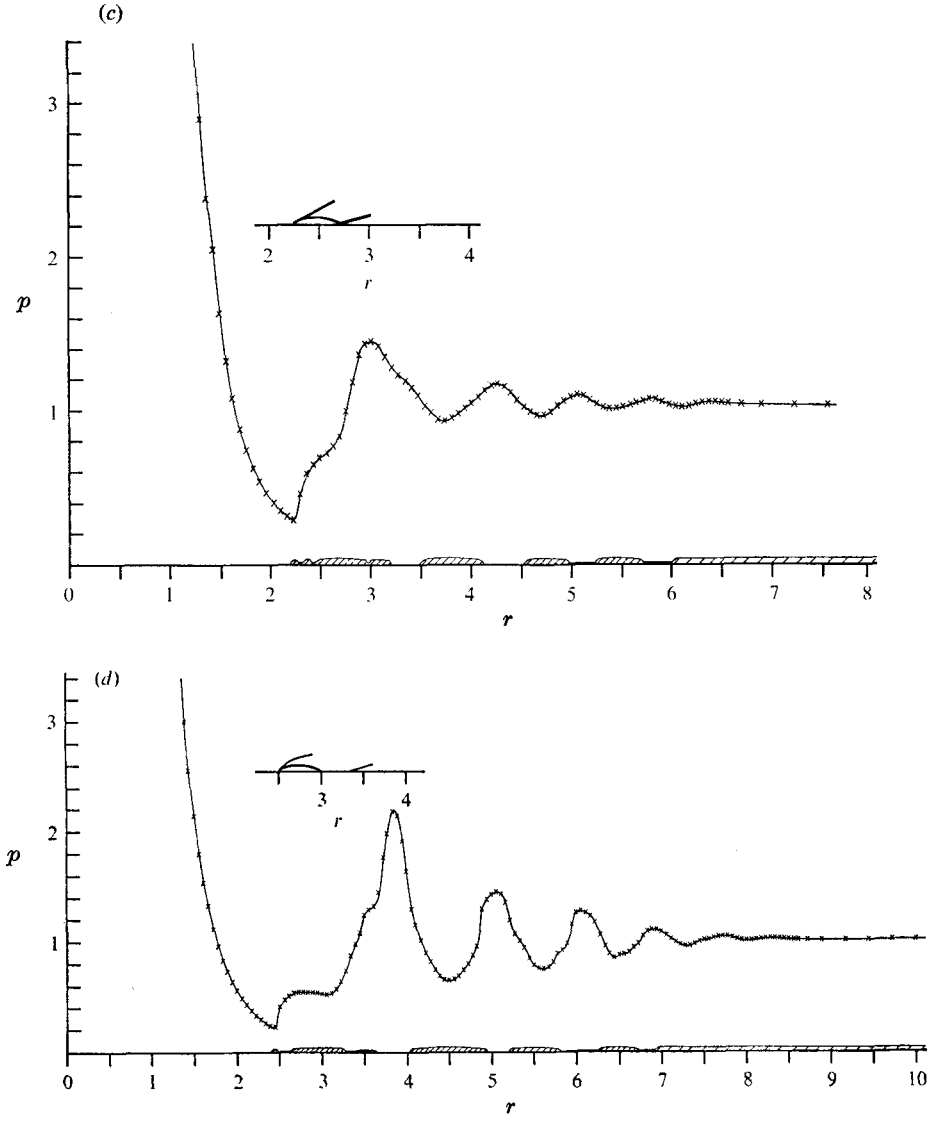

FIGURE 8. Wall-jet surface pressures for (*a*) $M_J = 1{\cdot}64$, (*b*) $M_J = 1{\cdot}76$, (*c*) $M_J = 2{\cdot}41$ and (*d*) $M_J = 2{\cdot}77$. The pressures are non-dimensionalized with respect to atmospheric pressure and the radial co-ordinate with respect to the jet radius.

the material which lies immediately inside them from flowing outwards. In the case of the first minimum, the velocities are very high and the shear stress ahead of the minimum is sufficient to remove the Dayglo. The possibility that the Dayglo deposits alter the wall-jet flow cannot be completely dismissed but this is felt to be unlikely, since the deposits are much thinner than the wall jet.

It is, perhaps, too much to expect that the structure of the Dayglo patterns in the region of the first minima of the $M_J = 2{\cdot}77$ and $M_J = 2{\cdot}41$ wall jets can be directly related to the rather complex pressure distributions measured in these regions. In the case of the 2·77 wall jet, the agreement is surprisingly close. The

contour representing the Dayglo patterns and drawn on figure 8 (*d*) is admittedly subjective; however, this contour was constructed before the pressure measurements were obtained and was therefore not influenced by a desire for agreement. The Dayglo deposits appear to consist of three parts, an initial narrow ring, corresponding to the initial very sharp pressure rise, a wider ring whose position agrees well with the separated region and a rather faint third ring corresponding to the region of reduced shear stress caused by the reattachment shock. The Dayglo patterns for the $M_J = 2{\cdot}41$ wall jet also show a complex structure behind the first minimum, indeed the complexity is greater than that seen in the pressure measurements. We are not able to explain this. However, it may be significant that this part of this wall jet was one of only two regions where significantly different Dayglo patterns were obtained from one test to another. This particular photograph is chosen for presentation because of its general high quality but the results of the three other tests which were conducted are in better agreement with the pressure distribution in this region, showing only two rings, one corresponding to the initial, sharp pressure rise and the other to the place where the boundary layer thickens. The other region where different results were obtained from different tests is the first ring of the $M_J = 1{\cdot}84$ wall jet. In figure 6 (*b*), this ring contains a small gap which has no counterpart in the pressure distribution of figure 9 (*b*). A second test with the same nozzle produced a ring at the same place and occupying the same interval, but without a gap.

A very limited amount of previous work has been done on the surface flow visualization of impinging supersonic jets. Greenwood (1969), using the nozzles employed in this work, observed naturally occurring oil and ice deposits; comparison of these with the present results shows that they occurred in the region of the first pressure rise. Donaldson & Snedeker (1971) used a mixture of grease and lampblack to investigate a stagnation bubble of the type discussed in §4.1. Their jet was produced by the underexpanded flow from a convergent nozzle, resulting in Mach numbers of the order of 1·9 upstream of the plate shock. A photograph of their surface flow patterns shows evidence of the separation bubble and also of a ring of deposit at a greater radial distance. Donaldson & Snedeker do not comment on this outer ring but if its position is non-dimensionalized by the jet radius at the shock, then it turns out to occupy the region $r = 2{\cdot}1$ to $r = 2{\cdot}6$. This may be compared to the positions of the first pressure rise in the present $M_J = 1{\cdot}76$ and $M_J = 2{\cdot}41$ wall jets, which are $r = 1{\cdot}9$ to $r = 2{\cdot}5$ and $r = 2{\cdot}4$ to $r = 3$ respectively. Belov *et al.* (1969) present results for a visualizing material (which they do not describe) used in conjunction with the underexpanded jet from a nozzle with an exit Mach number equal to 2. Their results show three or four rings of the type presented here. Belov *et al.* also measured boundary-layer velocity profiles for the same nozzle operated at a lower, but still underexpanded, pressure ratio. These measurements showed a region of flow separation. Quantitative comparison with the present results is not possible for the surface patterns, since the photograph by Belov *et al.* contains no scale, and is not easy for the separated flow because, not only is the jet structure different, but also the jet radius at the shock is not known. A rough comparison can be made by assuming that the jet radius is equal to that for a uniform flow at the ambient

pressure and supply stagnation pressure and then non-dimensionalizing the radial co-ordinate with respect to this value: the corresponding jet Mach number is 2·63. This gives a separated zone extending from approximately $r = 2{\cdot}3$ to $r = 2{\cdot}8$, which should be compared with the separation found in the present work at $M_J = 2{\cdot}77$, which occupies the approximate region $r = 2{\cdot}7$ to $r = 3{\cdot}1$. Although our results are consistent with those of Belov *et al.*, our interpretation is quite different. Belov *et al.* ascribe the regular pattern of surface flow rings to the existence of standing waves in the boundary layer, set up under the influence of turbulence from the shear layer. The evidence of the present paper supports an interpretation in terms of the inviscid wave structure rather than the standing wave model.

5. Approximate calculation of the near wall jet

This section presents a simple application of the method of characteristics to the near wall jet which, although somewhat crude, nonetheless reproduces the main features of the flow as far as the first recompression region and demonstrates the importance of the edge expansion in determining this part of the flow.

In the method used here, the proper characteristic equations for non-homentropic axisymmetric flow are used. However, the internal grid points are ignored and only boundary points are calculated. Some allowance for the curvature of the characteristics is made by representing them as circular arcs between the slopes calculated at the boundaries.

The boundaries of the region are the constant-pressure upper boundary of the wall jet, the solid surface, the sonic line and any part of the plate shock wave which lies between the sonic line and the jet edge. The position, flow direction and stagnation pressure on the solid surface are known and the Mach number is calculated; along the upper boundary, the Mach number and stagnation pressure are known, the flow direction is calculated and the position is constructed as a series of circular arcs between successive calculated points; the sonic line and shock waves are not known since no accurate solution for the shock layer exists. Such information as is available was described in §2 and was used to develop approximations for the shape and location of the sonic line and relevant part of the shock wave. The final forms of these approximations depend on the choice of a value for the Mach number M_E on the jet-edge streamline immediately downstream of the shock. The minimum possible value of M_E is unity and it was found possible to estimate its maximum possible value for each jet. These values were used as a guide in choosing the values of M_E to be used in the calculations. The stagnation pressure along the sonic line was assumed to vary linearly with perpendicular distance from the solid surface between the known values at the two ends of the line.

Since no internal grid points are calculated, the number of characteristics used only affects the accuracy of the calculated values through the construction of the constant-pressure upper boundary. It was felt that it was consistent with the level of approximation used to start with two characteristics from the jet edge; these were the initial and final characteristics of the expansion region. In some cases, a further characteristic was introduced from the foot of the sonic line.

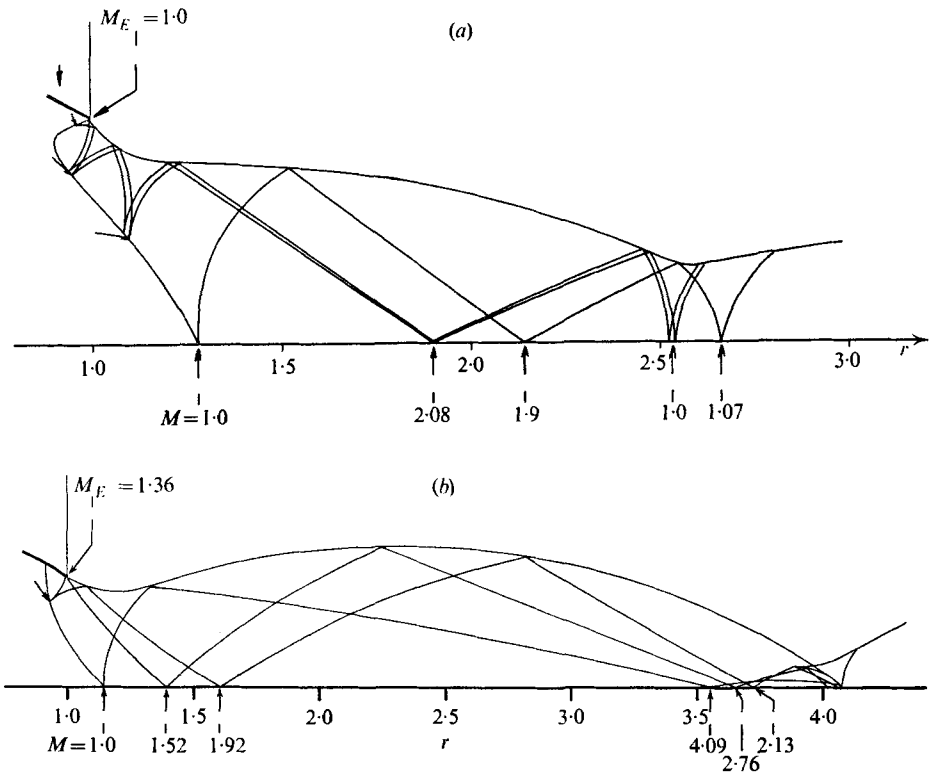

FIGURE 9. Wall-jet characteristics for (*a*) $M_J = 1{\cdot}64$ and (*b*) $M_J = 2{\cdot}77$.

The method just described was applied to wall jets for the nominal jet Mach numbers of the experimental nozzles. The results for two of the jets are presented in figures 9 (*a*) and (*b*); r is the radial distance in jet radii. The details of the figures should be interpreted with care: it is important to bear in mind that the internal lines represent characteristics, not waves, that the axisymmetric and non-homentropic effects can be strong and that flow quantities are known only at the ends of characteristics. A number of calculated surface Mach numbers are shown on the figures.

Figure 9 (*a*) shows the construction for the $M_J = 1{\cdot}64$ jet for an edge Mach number M_E of unity. The first point of minimum pressure occurs at $r = 1{\cdot}9$ and the subsequent recompression terminates at $r = 2{\cdot}51$; the corresponding values on the experimental pressure distributions are $r = 1{\cdot}9$ and $r = 2{\cdot}37$, respectively. The calculated value of the maximum surface Mach number is 2·08, compared with an experimental value of 1·73 (assuming a normal-shock value of the total pressure on the surface streamline). It is not possible to make a close comparison of the calculated wall-jet edge with that obtained experimentally because the wall-jet edge is not well defined on the shadowgraph picture. Such features as can be discerned from the shadowgraph are in agreement with the calculated jet edge. Repeating the calculation first using homentropic planar characteristics and then using homentropic axisymmetric characteristics shows that the effect

of the variation in entropy is small, as is to be expected at this jet Mach number, but that the axisymmetric effect is very considerable: the point of minimum pressure occurs at $r = 2{\cdot}5$ under the assumption of planar flow and the wall jet is much thicker, because the height for a given flow area no longer decreases with radial distance. Raising the jet-edge Mach number to its estimated maximum value of 1·1 slightly changes the appearance of the characteristics but makes no significant difference to the main features.

The main features of the calculation for the $M_J = 1{\cdot}84$ jet (not presented here) also show good agreement with the corresponding experimental results. In the case of the two higher Mach number jets, the accuracy of the calculated results is lower. The construction for the $M_J = 2{\cdot}77$ wall jet is presented in figure 9 (*b*). The first recompression is seen to occupy the radial interval 3·5–4·1, compared with an experimental range of 2·4–3·8. The calculated and experimental values of the maximum surface Mach number are 4·09 and 3·16 respectively. These overestimates of the maximum surface Mach number and of the value of its radial co-ordinate are probably due to the crudity of the characteristics mesh used since, in a more accurate computation, characteristics from the upper boundary in the initial part of the first recompression zone will converge on characteristics in the final part of the first expansion and reduce its extent, both in space and in terms of the maximum Mach number achieved. In any case, the construction becomes increasingly sensitive to errors as the Mach number increases, because of the decreasing values of most Mach angles. The shape of the upper boundary is in good general agreement with the impression gained from the shadowgraph picture (figure 4 (*d*)): even the striking reduction in wall-jet thickness in the vicinity of the first recompression can be discerned in the shadowgraph. It can be seen in figure 9 (*b*) that characteristics of the same family cross each other in the region of the first recompression and the construction loses its meaning. This is consistent with the experimentally observed formation of shock waves in this region.

Since even this highly approximate application of the method of characteristics has successfully reproduced several important features of the flow, it seems likely that a more complete computation, including internal points, would give good agreement with the experimental results as far as the first recompression. However, the accuracy will be limited by the significant thicknesses of the shear layer and the boundary layer and by the accuracy of the data available on the sonic line.

6. Conclusions

Detailed and accurate surface pressure distributions have been obtained covering the wall-jet regions of four supersonic nominally uniform jets. Shadowgraph and surface flow visualization pictures have also been obtained. The shadowgraph pictures are consistent with the pressure distributions. The surface flow visualization pictures show interesting patterns which are clearly related to the pressure distributions but whose detailed interpretation is, at this stage, partly speculative. The application of the method of characteristics in an

approximate manner reproduces a number of the features of the near wall jet which are observed experimentally.

The results show that the supersonic near wall jet is largely determined by the inviscid part of the flow field and that the dominant factor is the jet-edge expansion and its reflexions from the sonic line and the wall-jet boundaries. Further out, viscous effects become increasingly important and a constant-pressure shear flow is eventually established. The distance at which this occurs increases with the Mach number of the jet. The near wall jet consists of an alternating series of expansion and recompression regions, the strengths of which depend on the jet Mach number. For Mach numbers of 2·4 and above, the first recompression is sufficiently strong for shock waves to form and at a Mach number of 2·77, the boundary layer is observed to separate locally.

Pressure distributions obtained in the shock layer show that a stagnation bubble can occur and that its occurrence depends on factors such as the manner in which the nozzle is supplied with air. The available evidence suggests that the wall-jet region is largely independent of whether or not a bubble occurs in the shock layer.

REFERENCES

BELOV, I. A., GINZBURG, I. I., ZAZIMKO, V. A. & TERPIGOR'EV, V. S. 1969 *Heat & Mass Transfer (U.S.S.R.)*, **11**, 167.

DONALDSON, C. DU P. & SNEDEKER, R. S. 1971 *J. Fluid Mech.* **45**, 281.

GREENWOOD, R. N. 1969 The measurement of recovery temperature in the region of interaction of a supersonic jet with a flat plate. M.Sc. thesis, University of Bristol.

GUMMER, J. H. 1968 The interaction of a supersonic jet with a flat plate. M.Sc. thesis, University of Bristol.

GUMMER, J. H. & HUNT, B. L. 1971 *Aero. Quart.* **22**, 403.

HAYES, W. D. & PROBSTEIN, R. F. 1966 *Hypersonic Flow Theory*, vol. 1. Academic.

HENDERSON, L. F. 1966 *Z. angew. Math. Phys.* **17**, 553.

HUNT, B. L. 1972 *Aero. Quart.* **23**, 7.

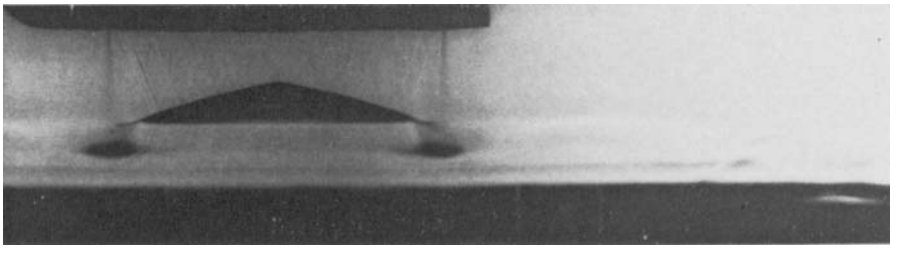

FIGURE 5. Shadowgraph of the $M_J = 2{\cdot}77$ jet on rig II.

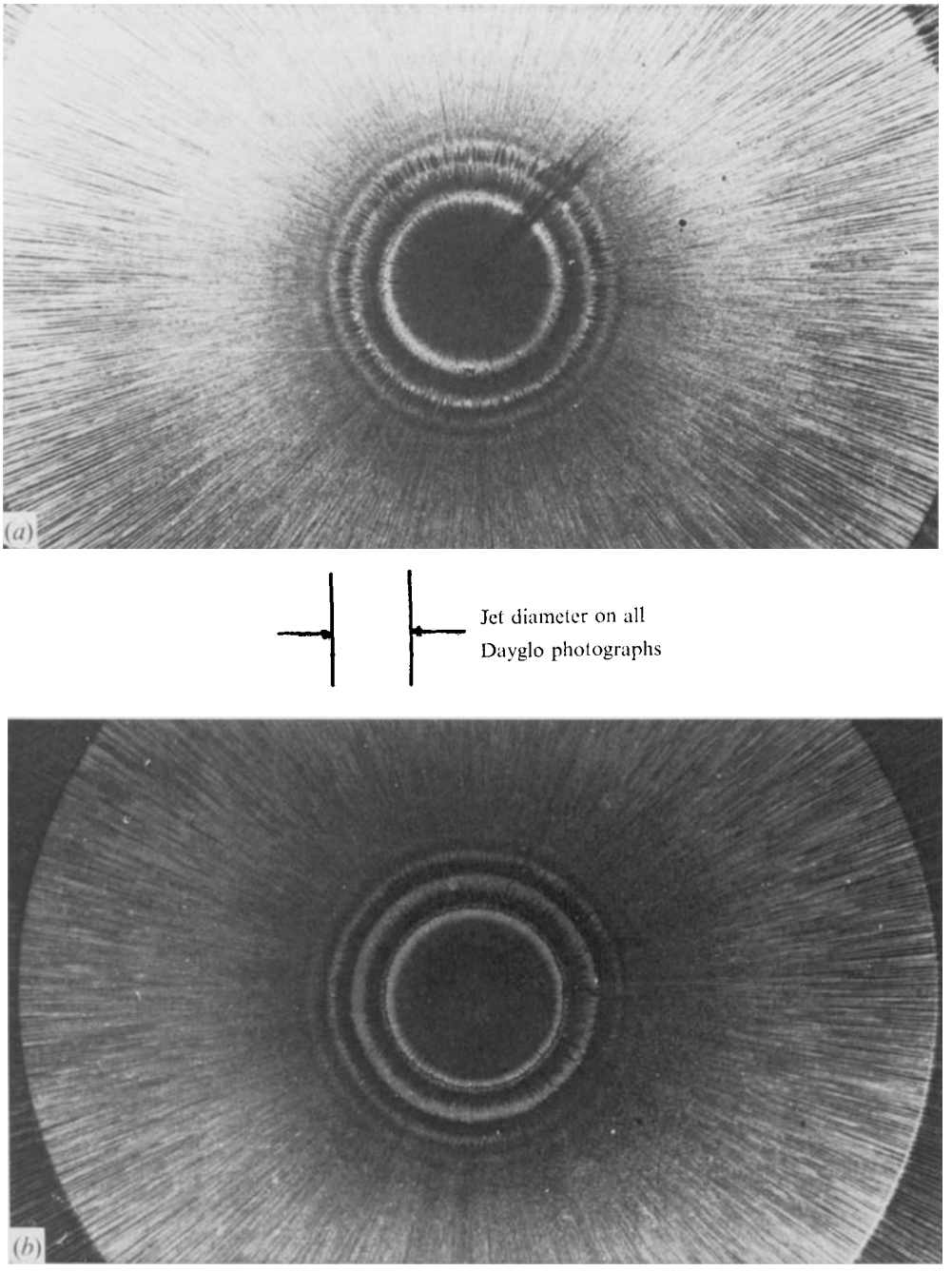

FIGURES 6 (*a*, *b*). For legend see facing page.

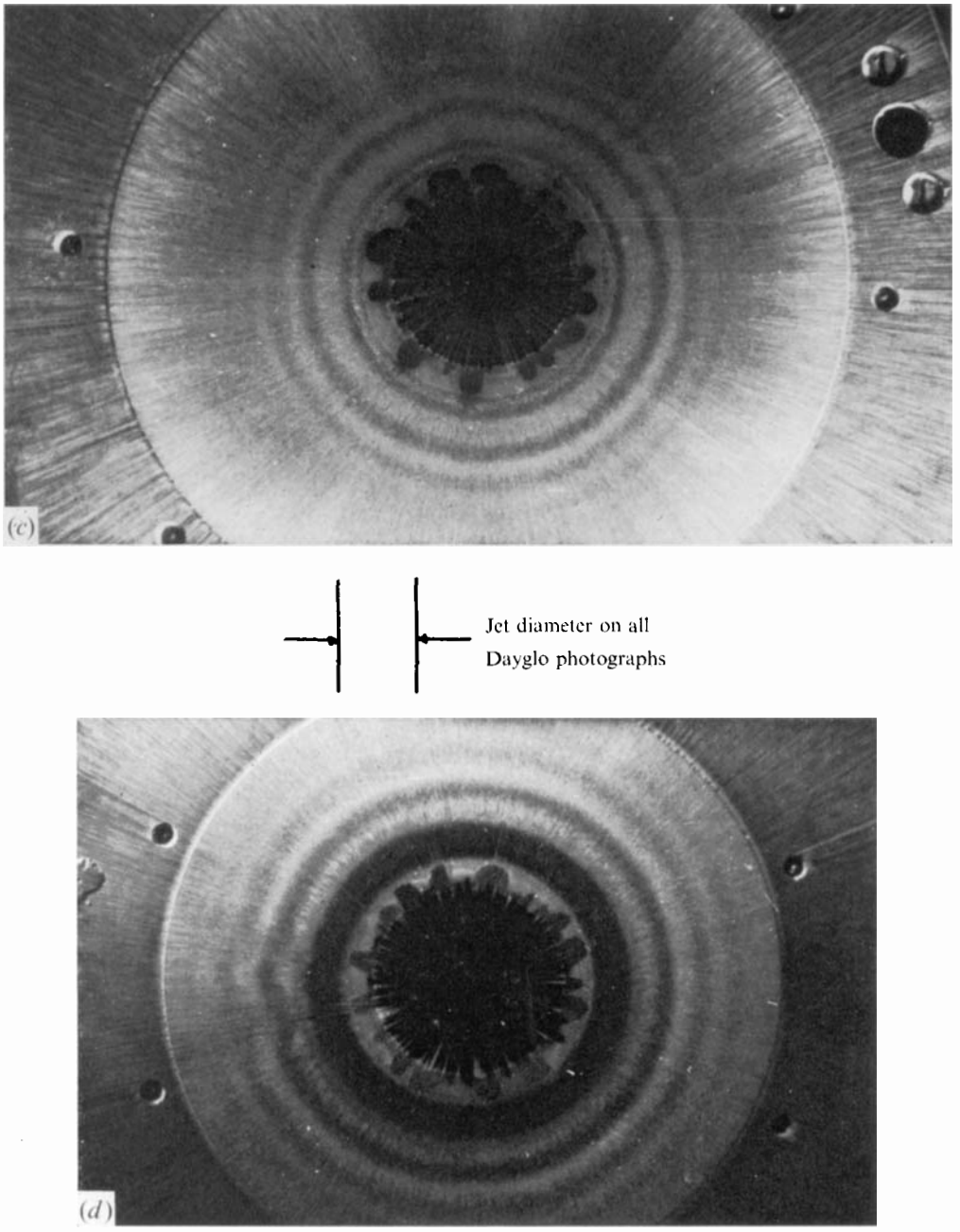

FIGURE 6. Surface flow patterns for (*a*) $M_J = 1{\cdot}64$, (*b*) $M_J = 1{\cdot}84$, (*c*) $M_J = 2{\cdot}41$ and (*d*) $M_J = 2{\cdot}77$.

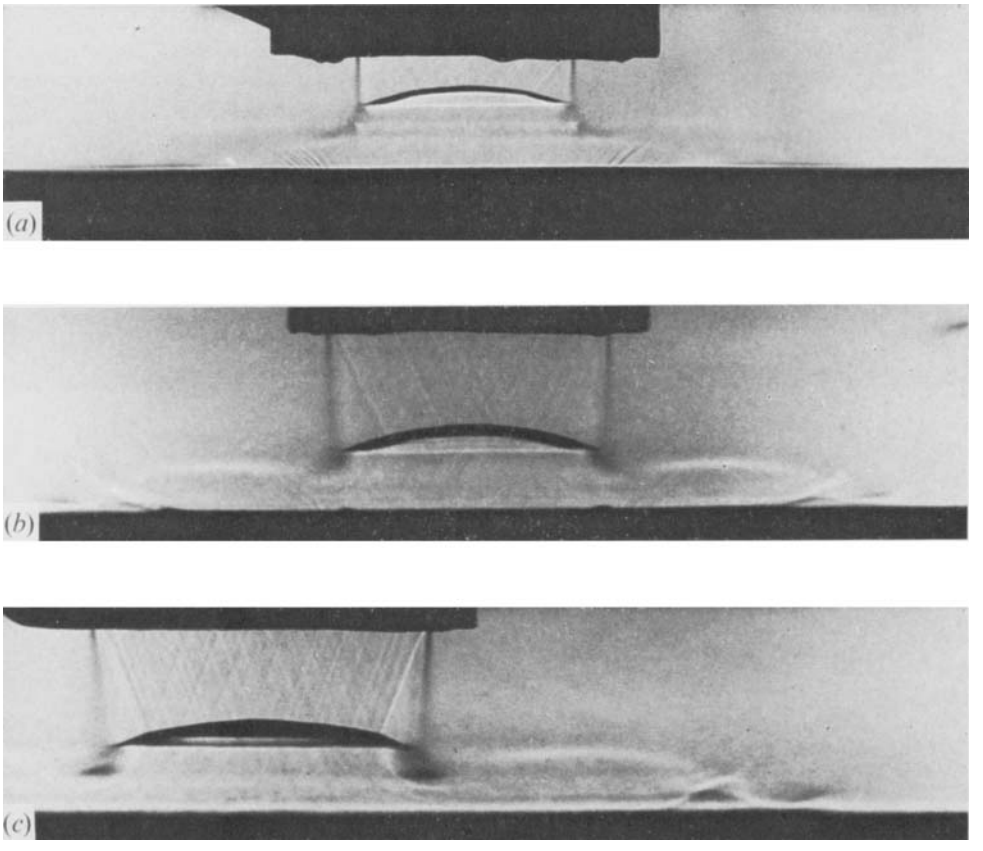

FIGURE 7. Shadowgraphs of (*a*) the $M_J = 1{\cdot}64$ jet, (*b*) the $M_J = 2{\cdot}41$ jet and (*c*) the $M_J = 2{\cdot}77$ jet.